Soft Matter

Accepted Manuscript

Volume 13
Number 45
7 December 2017
Pages 8341-8662

Soft Matter

rsc.li/soft-matter-journal

ISSN 1744-6848

PAPER
Kersten Baumgarten and Brian P. Tighe
Viscous forces and bulk viscoelasticity near jamming

ROYAL SOCIETY OF CHEMISTRY

rsc.li/soft-matter-journal

Modeling Dynamic Swelling of Polymer-Based Artificial Muscles

Shefik Bowen[1] and Daniel T. Hallinan Jr.[1,*]

[1]Florida A&M University-Florida State University (FAMU-FSU) College of Engineering, Department of Chemical & Biomedical Engineering and Aero-propulsion, Mechatronics, and Energy Center, Tallahassee, FL 32310.
*Corresponding author email: dhallinan@eng.famu.fsu.edu

Keywords

Diffusion, Migration, Actuation, Numerical Modeling, Crosslinked Network

Abstract

Polymer-based artificial muscles are lightweight, are flexible, can have variable stiffness, and provide actuation in applications in which heavy actuators are not feasible. Achieving device requirements, such as strain, strain rate, lifetime, achievable work, and efficiency, requires material and muscle geometry design. This study is motivated by the possibility of significant actuation from twisted and coiled polymer (TCP) fibers that rely on radial swelling to produce reversible work. Modeling the actuation of advanced polymers is essential for defining design metrics. An analytical thermodynamic expression based on Flory-Rehner Theory was combined with a numerical transport model in order to simulate transient swelling of a polymeric network driven by diffusion and migration. Radial swelling of polymer fibers was modeled, including parametric studies and comparison to experimental data. By increasing the transport distance, swelling is shown to increase the time to equilibrium, but this can be more than compensated by applying voltage to take advantage of ion migration/electroosmotic drag. This work indicates that, in addition to migration, dimensions smaller than 100 micrometers here are needed to achieve the sub-second response times of natural muscles. The impact of polymer swelling on transport in polymers is directly evaluated by locally accounting for the length increase of discrete elements due to solvent presence, which cannot be done analytically. Furthermore, strain and work done by swelling a TCP is modelled, and the benefit of anisotropic swelling and constant modulus is quantified.

Introduction

Based on the root words, an artificial muscle is a humanly contrived material attached at either end to a fixed point that contracts to cause or resist movement. A large enough force created by these muscles must be generated within a period of time similar to or smaller than times and forces seen in nature. Surpassing natural muscle actuation capabilities is a challenging but essential goal of artificial muscle research. Doing so will allow for mechanical enhancement in a variety of applications such as active prosthetics,[1, 2] robotics,[3, 4] and exoskeletons.[5]

Natural muscles achieve large actuation strains by taking advantage of a hierarchical design in which individual myosin-actin binding events generate small contraction via a filament sliding mechanism. Many such events within myofibril protein bundles contribute to the contraction of sarcomeres, many of which make up a muscle cell, also known as a muscle fiber. Muscle fibers are approximately 10 to 100 μm in diameter and 75 cm long.[6] They work in concert to generate approximately 10 N/cm^2 of tensile stress over roughly 50 microseconds.[7] Such complex

hierarchical design and complex cascade of actuation events cannot be practically implemented in polymeric artificial muscles with existing technology. A strain of at least 5% is needed to mimic natural muscles, whereby larger motion can be achieved using mechanical disadvantage, as in the human body.[6]

Actuation, i.e. change in dimension, can be achieved by numerous physical mechanisms such as molecular reorientation, thermal expansion, response to an applied field, and swelling due to solvent and/or ion transport.[8] Molecular reorientation occurs in natural muscles, in light-responsive materials, and in some conductive polymers with a change in oxidation state. Light-response is often achieved with a liquid crystalline moiety, such as azobenzene or cinnamic acid, that has large aspect ratio. Collective reorientation of the liquid crystalline moieties, especially when attached to a polymer or network, results in significant actuation if exposure to light of appropriate wavelength is possible. Thermal expansion has received the most attention and has been applied to nylon and polyethylene fibers. However, it is generally accepted that this approach yields poor energy-to-work efficiency. Similarly, response to an applied field, such as Maxwell stresses that occur when extremely high voltages are applied across an elastomer, are considered impractical in most applications. Polymer dimensions increase when they absorb solvent molecules. Interestingly, the solvent swelling approach can be combined with other mechanisms, such as thermal expansion or ionic doping of conductive polymers, in order to achieve large strains with relatively good rate.[9]

Diffusion of neutral molecules in polymers is described by Neogi.[10] Diffusion of solvents with polymer relaxation has been studied in Cartesian coordinates,[11] but diffusion and relaxation were handled separately and empirically. Hallinan *et al.* reported the diffusion, sorption, and swelling of methanol and water in Nafion.[12] The concentrations of methanol and water were monitored using Fourier Transform Infrared – Attenuated Total Reflectance (FTIR-ATR) spectroscopy. The size and type of solute, as well as the external solution concentration, affect not only the magnitude of the diffusion coefficient, which dictates swelling rate, but also the amount of sorption, which dictates swelling amount.[13] The glassy or rubbery nature of the polymer has been shown to affect the dynamics of sorption-induced swelling as well, where a delay is observed in glassy polymers.[14] There is a long history of studying swelling of crosslinked polymer networks, due in part to the reversible nature of the swelling. Early work measured dynamic swelling[15] and modeled solvent transport analytically,[16] but the effect of swelling on transport has not been explicitly accounted for.

Composite networks can exhibit synergistic improvements over networks composed of a single chemistry. For example, polymer hydrogel composites containing natural fibers (cellulose from cotton) showed improvement over simple polymer hydrogels.[17] The natural fiber increased the volumetric swelling of poly(acrylic acid) (PAA), a polyelectrolyte, and it stabilized the PAA chains by acting as a crosslinker, which improved reversibility of swelling and deswelling by water. Loosely crosslinked ionic polymer networks (i.e. with low crosslink density) were studied by Gao *et al.* in 2013.[18] These hydrogels contained hydrophilic groups such as $-COO^-$, $-COOH$ and $-CONH_2$, all with varied hydrophilicities within poly(acrylic acid-co-acrylamide)/montmorillonite. A comparison was made between distilled water and a 0.9% NaCl solution. Due to neutralization of acrylic acid, the salt solution resulted in restricted swelling. These examples demonstrate that ion containing materials are of interest for swelling by green

solvents, such as water.

Electric fields are another stimulus that can modulate the swelling of charged polymers. Ion migration can induce bending or linear actuation in ionic polymer metal composites (IPMCs).[19] Swelling is induced by sorption and/or transport of solvent and ions in the presence of an electric field.[20] IPMCs are improved by using low-vapor-pressure polar solvents like propylene carbonate and ionic liquids,[21-23] but they suffer from poor reversibility due to the transient nature of their actuation mechanism. Another class of polymers that conduct electrons or holes rather than ions are electroactive polymers (EAPs). EAPs can be oxidized and reduced at electrodes, whereby applied voltage induces actuation via conformational changes of the polymer that are caused by redox reactions. A commonly studied EAP is polyaniline (PANI).[24] In fact, electrochemical reactions have been combined with bulk reactions (via pH control) to realize actuation in chitosan/polyaniline/carbon nanotube composites.[25] Polypyrrole is another EAP that can participate in redox reactions.[26] If driven at sufficiently high voltage, irreversible degradation of EAPs occurs.[27] Although degradation can be important, it is not accounted in the model designed in this study. This work is tailored for hydrophilic and ion-containing polymers, building on the strong foundation available for modeling diffusion and migration of solvent and ions in polymers.

Twisting and coiling of fibers is perhaps the most promising approach to achieve the large strains needed for artificial muscles to surpass the performance of natural muscles. Fibers are usually formed by drawing a polymer melt into a filament. Drawing is a classic technique that dramatically increases the axial strength of a polymer by aligning the chains preferentially in the axial direction.[28] This also acts to increase the degree of crystallinity if it is a semicrystalline polymer. The preferential chain alignment results in anisotropic swelling (and thermal expansion), whereby changes in the radial direction are much more significant than those along the filament length.[29] These filaments can be bundled (if desired) and twisted as individual filaments or bundles. If a sufficient amount of twist is inserted, the mechanical energy is minimized by converting some of the twist into writhe, which results in coils that look like those in a spring. Homochiral twisted and coiled actuators (TCAs) convert radial expansion into much larger contraction along the axis of the twist/coil. This occurs due to the mechanics and geometry, and the theory describing the effect is relatively well developed,[30, 31] although agreement with experiment varies from good[31] to rather poor.[32] In any case, modeling of expansion/contraction in the radial direction is key.

TCAs have been constructed from a variety of designs, such as single solid filaments, filament bundles, weaves, 2D braids and 3D braids. Bundles were found to have low efficiency where the authors recommended that a ratchet-and-locking mechanism be employed to increase the efficiency.[32] The low efficiency was due to the bundles being actuated by thermal expansion.[31-33] Conductive material can also be added, namely Ag, Pt, Au or Carbon. It can be combined with a polymer network, e.g. in core-shell structures, to provide a means for electrical heating, electrochemical reaction, or electromotive ion migration.[33] TCAs have been constructed from materials such as nylon 6, nylon 6,6 and polyethylene[32], as well as carbon nanotube yarns filled with guest substituents such as poly(dimethylsiloxane) (PDMS)[31] and paraffin wax.[34] Water diffusion in nylon 6 was studied by Kojima *et al.* in 1993.[35] This was combined with thermal expansion by Haines *et al.* in 2014 where a coiled polymer muscle made of nylon 6 fishing line was driven at 1 Hz by switching between cold (~25 °C) and hot (95 °C)

water, causing 12% reversible actuation under a 0.5-kg load (8.4 mPa).[32] There have been several studies using thermal expansion with TCAs with various temperature-control mechanisms, reviewed by Lamuta *et al.*[31] In their study, electrical-resistance-based heating was used, and a transient continuum model was developed specifically for thermal actuation of TCAs. In addition to the poor efficiency of thermal actuation, cooling tends to be slow. Swelling based on solvent and/or ion transport, on the other hand, can surpass the Carnot efficiency limit.[36] Due to the potential benefits of this actuation mechanism, a solvent/ion transport model has been developed and is reported herein.

This study models transport-based swelling induced by diffusion and migration. It also handles cylindrical shape, which better simulates diffusion in an artificial muscle fiber. Swelling coupled to transport is nontrivial, and, to the best of our knowledge, cannot be handled analytically with finite boundary conditions. Scaling with a dynamic length scale cannot be used due to the gradient of swelling (through the fiber radius) during the transient period before equilibrium is reached. In addition to these advancements in modeling artificial muscle actuation, this study adds migration to the mathematical model, which accounts for the effects of electrical potential gradient (i.e., electric field) on the swelling of polymers. In other words, the model presented here handles not only diffusion-based swelling of polymer fibers by neutral molecules, but also migration-based swelling.

Materials and Methods
The polymeric fiber/filament that is modelled in this work has an interaction parameter of 0.56 with water which is similar to the electroactive polymer sulfonated poly(ether ether keytone) (SPEEK) infiltrated by methylamine acting as the solvent. The diameter of 0.1 mm is similar to a fishing line rated for 1 kg and on the same order as a natural muscle fiber. The fiber length is much greater than its radius (nominally 1 m in this work). In TCA's the radius change is the important factor that affects actuation and thus is the main focus in this study. Uncoiled fiber length is important to measure and observe when applying twists and inducing coils that shorten the axial length of the TCA. Transient diffusion models in Cartesian and cylindrical coordinates are used. The outer boundary condition is determined by thermodynamics, and the inner boundary is symmetric (or has no flux). Existing TCA theory is used to convert the rate and amount of radial swelling to axial contraction of the coil.

Thermodynamics
In this work, key factors are derived from Flory-Huggins Theory that considers the combinatorial entropy of mixing polymer and solvent molecules.[37] The elastic response of the network is also considered.

$$\Delta G_{sw} = \Delta G_{mix} + \Delta G_{el} \quad (1)$$

Here, ΔG_{sw} is the Gibbs free energy of swelling that is the sum of the Gibbs free energy change due to mixing (ΔG_{mix}) and the Gibbs free energy change due to stretching of elastically active network chains (ΔG_{el}) in a cross-linked polymer network. ΔG_{mix} promotes swelling, while ΔG_{el} opposes swelling.

The Gibbs free energy change due to mixing is defined by:

$$\Delta G_{mix} = kT[N_1 ln(\phi_1) + N_2 ln(\phi_2) + \chi N_1 \phi_2] \qquad (2)$$

where k is the Boltzmann constant, T is temperature, N_1 is the number of solvent molecules, N_2 is the number of polymer molecules, and χ is the Flory-Huggins polymer-solvent interaction parameter, while ϕ_1 is solvent volume fraction, $\frac{V_{solvent}}{V_{swollen\ polymer}}$, and ϕ_2 is polymer volume fraction, $\frac{V_{dry\ polymer}}{V_{swollen\ polymer}}$.

In the case of a highly crosslinked system with very little separate, uncrosslinked polymer molecules, N_2 approaches zero and the equation reduces to:

$$\Delta G_{mix} = kT[N_1 ln(\phi_1) + \chi N_1 \phi_2] \qquad (3)$$

Regarding the Gibbs free energy change when elastic expansion of the crosslinked structure occurs, ΔG_{el} can be defined as:

$$\Delta G_{el} = kT \frac{N_{bc}}{2}[3\alpha_s^2 - 3 - ln\alpha_s^3] \qquad (4)$$

where N_{bc} is the number of crosslinks per chain, and α_s is the linear deformation factor $\left(\frac{R}{R_i}\right)$. An assumption in Equation 4 is that deformation is isotropic and linear. When an equilibrium condition occurs, the difference between the chemical potential of the solvent within the swollen polymer (μ_s) and the chemical potential of the pure solvent (μ_s^0) in which the networked polymer is immersed is described by

$$\mu_s - \mu_s^0 = N_A\left(\frac{\partial \Delta G_{mix}}{\partial N_1}\right)_{T,P} + N_A\left(\frac{\partial \Delta G_{el}}{\partial \alpha_s}\right)_{T,P}\left(\frac{\partial \alpha_s}{\partial N_1}\right)_{T,P} \qquad (5)$$

where N_A is Avogadro's number. To find solutions to the partial derivatives, first consider that:

$$\alpha_s^3 = \frac{1}{\phi_2} = \frac{V_{swollen\ polymer}}{V_{dry\ polymer}} = \frac{V_{dry\ polymer} + \frac{N_1 \nu_1}{N_A}}{V_{dry\ polymer}}, \qquad (6)$$

where ν_1 is the molar volume of the solvent. In the case of water, $\nu_1 = 18$ cm^3/mol at 25 °C. Volume additivity is assumed and therefore:

$$\left(\frac{\partial \alpha_s}{\partial N_1}\right)_{T,P} = \frac{\nu_1}{3\alpha_s^2 V_{dry\ polymer} N_A} \qquad (7)$$

After evaluating the partial derivatives and counting moles rather than molecules, we obtain:

$$\mu_1 - \mu_1^0 = RT\left[ln(1 - \phi_2) + \phi_2 + \chi \phi_2^2 + \nu_1\left(\frac{N_{bc}}{V_{dry\ polymer}}\right)\left(\phi_2^{1/3} - \frac{\phi_2}{2}\right)\right] \qquad (8)$$

At an equilibrium swollen state,

$$\mu_1 - \mu_1^0 = 0 \quad (9).$$

Using a molar basis, $N_{bc} = \frac{M_n}{M_c}$ and $\bar{v} = \frac{V_{dry\ polymer}}{M_n}$, where M_n is the number-averaged molecular weight of the polymer and M_c is the molecular weight between crosslinks.

$$-\left[\ln(1-\phi_2) + \phi_2 + \chi\phi_2^2\right] = \left(\frac{v_1}{\bar{v}M_c}\right)\left(1 - 2\frac{M_c}{M_n}\right)\left[\phi_2^{1/3} - \frac{\phi_2}{2}\right] \quad (10)$$

The term $2\frac{M_c}{M_n}$ accounts for the fact that chain ends are not effective crosslinks. After rearranging, the Flory-Rehner [38] equation is obtained:

$$\frac{1}{M_c} = \frac{2}{M_n} - \frac{\frac{\bar{v}}{v_1}\left[\ln(1-\phi_2) + \phi_2 + \chi\phi_2^2\right]}{\left[\phi_2^{\frac{1}{3}} - \frac{\phi_2}{2}\right]}. \quad (11)$$

Variables are defined in the nomenclature section.

An iterative method was used to solve for ϕ_2 at equilibrium, and thereby the volume ratio, which is $\frac{1}{\phi_2}$. Adjusting χ alters how much the polymer will swell and is related to the work that can be done by the artificial muscle fiber. Thus, the final swollen state is known based on the properties of the polymer and solvent, as well as their interaction parameter. What remains is to determine the time it takes to achieve the swollen state.

The parameters in the model can be adjusted to represent a myriad of crosslinked polymer/solvent combinations, including neutral polymers, ionically charged polymers, or conductive electroactive polymers with water, organic solvents, or ionic liquids. It should be noted that the thermodynamic theory does not technically capture polar and ionic interactions, but an effective chi parameter is commonly used to empirically quantify charged polymer-solvent interactions. For charged systems, eq. 11 would lose its connection to first principles, but would nonetheless maintain empirical functionality for modeling solvent-based swelling of crosslinked networks.

Transport

The study of diffusion in polymer networks requires the consideration that these polymers are in solid or gel state. Due to their solid-like nature, convection can be neglected. However, migration must be included when there are charged species present and a voltage is applied across the sample. This ability to model and analyze the differences when an electromotive force (EMF) is applied will be crucial to the development of specialized combinations of swelling agents and muscle fibers. The electric force per Coulomb on an ion is the product of the electric field (E) and the ionic charge, z_i, of the swelling agent. The flux of solvent/ion in a polymer sample (i.e. solute) is given by the Nernst-Planck Equation, which assumes that there is no homogeneous reaction:[39]

$$N_i = C_i\mathbf{v} - D_i\nabla C_i + z_i u_i \mathcal{F} C_i \mathbf{E}, \qquad (12)$$

where N_i is the flux of species i. The electric field, $\mathbf{E}$, is the negative of the gradient of potential,

$$\mathbf{E} = -\nabla\Phi. \qquad (13)$$

Assuming that convective flux is not present,

$$C_i\mathbf{v} = 0. \qquad (14)$$

In dilute solution, $D_i = R_{gas}Tu_i$, where u_i is the molar mobility of the ion. Inserting the Nernst-Planck Equation into a mass conservation equation and assuming constant diffusion coefficient yields

$$\frac{dC_i}{dt} = D_i\left[\nabla^2 C_i + \frac{z_i\mathcal{F}}{R_{gas}T}\nabla\cdot(C_i\nabla\Phi)\right].(15)$$

where i represents the solute.[39] Constant diffusion coefficient is a common assumption that has been shown to hold in systems such as Nafion/water,[40] but it is not universal. Exponential increase of diffusion coefficient with increasing solute concentration is a common empirical expression used to capture more mobile environment in highly swollen networks.[10] One of the advantages of the numerical (finite difference) model used in this work, is that such concentration dependence of diffusion can be easily handled.[41] For simplicity and due to similarity to polyelectrolyte-water systems, a constant diffusion coefficient is used in this work. When no electric field exists, the second term on the right-hand side of equation 15 is zero. Dropping subscripts, the 1-dimensional governing equation for a slab with no electric field is

$$\frac{\partial C}{\partial t} = D\left[\left(\frac{\partial}{\partial x}\left(\frac{\partial C}{\partial x}\right)\right)\right]. \qquad (16)$$

The cylindrical case for diffusion in the radial direction only is

$$\frac{\partial C}{\partial t} = D\left[\frac{1}{r}\left(\frac{\partial}{\partial r}\left(r\frac{\partial C}{\partial r}\right)\right)\right]. \qquad (17)$$

Using water as an example, diffusion coefficients of water in various polymers are reported in Table 1. In condensed phases, diffusion coefficients cannot be accurately predicted and must instead be found from best fits to experimental data. The diffusion coefficient used in this study is $D = 1\times10^{-7}\frac{cm^2}{s} = 1\times10^{-5}\frac{mm^2}{s}$, and the temperature is taken to be $T = 298\ K$.

Table 1. Diffusion coefficients of water in various polymer films from literature.[42-44]

Polymer	D $(cm^2\ s^{-1})$	T (°C)	Reference
poly(N,N-dimethylacrylamide)	1.10×10^{-8}	25	[42]

poly(N-vinylpyrrolidone) (PVP)	1.18×10^{-8}	25	[42]
poly(vinyl alcohol) (PVA)	2.24×10^{-12}	25	[42]
polyimide (Upilex)	0.10×10^{-8}	25	[42]
low-density polyethylene (LDPE)	7.42×10^{-8}	25	[43]
polyethylene terephthalate (PET)	0.56×10^{-8}	25	[43]
polyethylene (PE)	2.00×10^{-7}	25	[43]
Nafion 117	7.50×10^{-7}	30	[44]

In order to implement a numerical transport model, the governing equation must be discretized. In Cartesian coordinates the discretized governing equation (eqn 16) is

$$\frac{\Delta C(j,k)}{\Delta t} = D\left[\frac{\Delta}{\Delta x(j,k)}\left(\frac{\Delta C(j,k)}{\Delta x(j,k)}\right)\right] \quad (18)$$

where j is the space index, and k is the time index. The indices are written on the space step size in order to account for swelling, as will be made apparent shortly. In terms of a Forward Time-Centered Space (FTCS) finite difference, the concentration at the next step in time is explicitly calculated based on the known concentration, diffusion coefficient, time step size, and space step size.

$$C(j,k+1) = C(j,k) + \left(\frac{D\Delta t}{(\Delta x(j,k))^2}(C(j+1,k) - 2C(j,k) + C(j-1,k))\right). \quad (19)$$

The cylindrical version of equation 19, which better suits a fiber, in discrete form is

$$\frac{\Delta C(j,k)}{\Delta t} = D\left[\frac{1}{r(j,k)}\left(\frac{\Delta}{\Delta r(j,k)}\left(r(j,k)\frac{\Delta C(j,k)}{\Delta r(j,k)}\right)\right)\right] = D\left[\left(\frac{\Delta}{\Delta r(j,k)}\left(\frac{\Delta C(j,k)}{\Delta r(j,k)}\right)\right) + \frac{1}{r(j,k)}\left(\frac{\Delta C(j,k)}{\Delta r(j,k)}\right)\right]. \quad (20)$$

In terms of FTCS it is explicitly

$$C(j,k+1) = C(j,k) + D\Delta t\left(\frac{C(j+1,k) - 2C(j,k) + C(j-1,k)}{(\Delta r(j,k))^2} + \frac{1}{r(j,k)}\left(\frac{C(j+1,k) - C(j-1,k)}{2\Delta r(j,k)}\right)\right). \quad (21)$$

The stability criterion from Carnahan, 1969,[45] for one-dimensional FTCS is

$$\Delta t < 0.5 * \frac{\Delta x^2}{D}. \quad (22)$$

To be certain, we used the following to stay well within the stability range:

$$\Delta t = 0.01 * \frac{\Delta x^2}{D} \quad (23)$$

Concentration in molarity is related to volume fraction via molar volume of the component, which is a constant, i.e., $C_i = \phi_i/v_i$. Thus, the transport equations are equivalently expressed in terms of molarity or volume fraction. Either representation assumes that total concentration is approximately constant, which is a reasonable assumption if volume additivity holds and if the

molar volume of polymer segments and solvent are sufficiently similar. Volume additivity was assumed for the thermodynamic development. During swelling, the difference between the final total concentration of solvent swollen polymer and initial total concentration of dry polymer is

$$C_{total}(t \to \infty) - C_{total}(t=0) = \frac{\phi_1}{v_1} - \frac{\phi_1}{v_2}, \qquad (24)$$

which shows that the error is related to the molar volumes of the species. In addition to assuming volume additivity, the model will proceed with the assumption of equal molar volumes of polymer segments and solvent.

The benefit of using volume-fraction-based concentration is that it can be used to account for dynamic swelling. Assuming that no polymer dissolves during the swelling process, all addition of solvent leads to an increase in total volume that is inversely equal to the polymer volume fraction. As shown in equation 25, the increase in volume is handled in a discretized fashion at each numerical node where the step size is scaled by the linear swelling.

$$\Delta r(j,k) = \left(\frac{1}{1 - \phi_1(j,k)}\right)^{1/3} \Delta r(j,0) \qquad (25)$$

The initial step size, $\Delta r(j,0)$, is chosen to be 0.001 mm for the dry polymer at time zero ($k=0$) when $\phi_1(j,0) = 0$. Note that going forward C and ϕ_1 are used interchangeably.

In this initial model, water molecules are considered to have a charge of +1. This could, for example, be due to electroosmotic drag caused by the transport of protons in the form of hydronium, H_3O^+.[46-48] The presence of Eigen ions, $H_5O_2^+$, or higher-order hydrated proton species would require an adjustment to the value of z. The value of mobility in equation 15 could be modified to consider other ions,[49] but a rigorous approach would need to account for the presence of oppositely charged counter-ions, if they are mobile.[50] When considering the effect of an electric field on a fiber's uptake of solvent, the second term of equation 15 was retained to account for the migration of solvent/ions, which can be written

$$\frac{\partial C(j,k)}{\partial t} = D\left[(\nabla^2 C) + \frac{z\mathcal{F}}{R_{gas}T}(C\nabla^2\Phi + \nabla C \cdot \nabla\Phi)\right]. \qquad (26)$$

Here we assume electroneutrality throughout the sample, $\nabla^2\Phi = 0$. Moreover, we treated the gradient of potential, $\nabla\Phi$, as a constant. This makes the final Cartesian model

$$\frac{\Delta C(j,k)}{\Delta t} = D\left[\left(\frac{\Delta}{\Delta x(j,k)}\left(\frac{\Delta C(j,k)}{\Delta x(j,k)}\right)\right) + \frac{z\mathcal{F}}{R_{gas}T}\left(\frac{\Delta C(j,k)}{\Delta x(j,k)}\nabla\Phi\right)\right], \qquad (27)$$

and the final cylindrical model

$$\frac{\Delta C(j,k)}{\Delta t} = D\left[\frac{1}{r(j,k)}\left(\frac{\Delta}{\Delta r(j,k)}\left(r(j,k)\frac{\Delta C(j,k)}{\Delta r(j,k)}\right)\right) + \frac{z\mathcal{F}}{R_{gas}T}\left(\frac{\Delta C(j,k)}{\Delta r(j,k)}\nabla\Phi\right)\right]. \qquad (28)$$

In terms of FTCS, the explicit Cartesian expression is

$$C(j,k+1) = C(j,k) + D\Delta t\left(\frac{C(j+1,k) - 2C(j,k) + C(j-1,k)}{(\Delta x(j,k))^2} + \frac{z\mathcal{F}}{R_{gas}T}\left(\frac{C(j+1,k) - C(j-1,k)}{2\Delta x(j,k)}\nabla\Phi\right)\right), \quad (29)$$

and the explicit cylindrical expression is

$$C(j,k+1) = C(j,k) + D\Delta t$$
$$\left(\frac{(C(j+1,k) - 2C(j,k) + C(j-1,k))}{(\Delta r(j,k))^2} + \left(\frac{(C(j+1,k) - C(j-1,k))}{r(j,k)\,2\Delta r(j,k)}\right) + \left(\frac{z\mathcal{F}}{R_{gas}T}\right)\frac{C(j+1,k) - C(j-1,k)}{2\Delta r(j,k)}\nabla\Phi\right) (30).$$

Since electrolysis occurs at and above 1.23 V in aqueous solvents, [51] a value of $\nabla\Phi = 12.3$ V/mm was included in the range of potential differences used for simulations of polymers actuated with diffusion and migration. Any magnitude of electric field can be analyzed, and a range is shown in the results.

Boundary Conditions
The outer boundary is defined by the equilibrium value of ϕ_2 that comes from the solution to Flory-Rehner Theory (eq. 11).

$$C(R) = 1 - \phi_2 \quad (31)$$

The position of the outer boundary, R, is the sum of all the discrete space steps, swollen according to Equation 25. In other words, R is a function of the transient solvent volume fraction throughout the control volume, but the solvent volume fraction at the outer boundary is constant and determined by thermodynamics.

For an artificial muscle that does not have electrodes and is not of sheath-run construction, the inner boundary occurs at r or $x = 0$. This is the central plane of a slab in Cartesian coordinates and the central axis of a fiber in cylindrical coordinates. In both cases, symmetry applies here. For an artificial muscle with an impermeable core or an inner electrode that is not consuming the solvent, the inner boundary occurs at a non-zero position, where there is no flux. This was the case for cylindrical simulations in this work, i.e., $R_{ii} = 0.01$ mm. For all Cartesian calculations the inner boundary is $R_{ii} = 0$. Regardless, symmetry and no-flux boundary conditions yield the same mathematical expression.

$$\nabla C(R_{ii}) = 0 \quad (32)$$

Due to symmetry or the impermeable nature of the core, swelling does not affect the position of the inner boundary, i.e., R_{ii} is a constant. This boundary condition is implemented in the numerical model by defining an imaginary node that enforces the no-flux condition.

$$C(R_{ii} - \Delta r(0,k)) = C(R_{ii}) \quad (33)$$

Thus, equation 29 or 30 in conjunction with equations 11, 31, and 33 constitute the complete thermodynamic and transport description of transient 1D diffusion and swelling. The parameters used to evaluate these models are reported in Table 2, and the initial, boundary, and equilibrium conditions are presented in Table 3.

Table 2. Parameter values used in model.

Parameter	Value	Units
v_1 (molar volume of solvent)	18	cm^3/mol
M_n (number avg molecular weight)	200,000	g/mol
M_c (molecular weight per crosslink)	1,000	g/mol
ρ (density of polymer)	1.45	g/cm^3
$\frac{1}{\phi_2}$ (volume ratio)	2.77	-
D (diffusion coefficient)	1.0×10^{-5}	mm^2/s

Table 3. Initial, boundary, and equilibrium conditions.

Initial Condition	Cartesian	Cylindrical
@$t = 0$,	$C(x,0) = 0$	$C(r,0) = 0$
Boundary Conditions		
Inner	$\nabla C(0,t) = 0$	$\nabla C(R_{ii},t) = 0, R_{ii} = 0.01$ mm
Outer	$C(X(t),t) = 1 - \phi_2, X_i = 0.1$ mm	$C(R(t),t) = 1 - \phi_2, R_i = 0.1$ mm
Equilibrium Condition		
$Time_{final} = 3 * t_d =$	$3 * \dfrac{\left((\phi_2)^{-1/3} X_i\right)^2}{D}$	$3 * \dfrac{\left((\phi_2)^{-1/3} R_i - R_{ii}\right)^2}{D}$
@$t = Time_{final}$,	$X = (\phi_2)^{-1/3} X_i = V_{ratio}^{1/3} X_i$	$R = (\phi_2)^{-1/3} R_i = V_{ratio}^{1/3} R_i$

IV. Artificial Muscle Performance Metrics

1. Actuation stroke

Radial swelling of a coiled fiber is converted to axial stroke if the TCA is prevented from rotating. According to Love's theory[52], the change of fiber twist can be used to give the fiber stroke as:

$$\frac{\Delta L}{L} = \frac{l_a^2 \Delta U}{LN}, \quad (34)$$

where L is the unloaded coil length, N is the number of coils, l_a is the fiber length in the coil, and ΔU is the change of number of turns.

$$\Delta U = \frac{\Delta \tau}{2\pi} \quad (35)$$

where $\Delta \tau$ is the change of twist in radians. This does not make explicit how TCA actuation depends on fiber radius. So, it is more convenient to consider that linear actuation in a coil is due to the change in coil angle, β, with radial swelling.

$$\beta = cos^{-1} \left| \frac{1}{(EI - GJ)} \left(\frac{nEIGJ}{\sqrt{EI\mathbf{F}}} - 2GJ \right) - 1 \right| \quad (36)$$

The inserted twist (in radians) per fiber length is $n = \Delta\tau/l_a$. The tensile modulus is E; the second moment of fiber area is I; the shear storage modulus is G; the polar second moment of fiber area is J; and the applied load is $\mathbf{F}$.[31] The coil angle is measured from the coil axis to the centerline of the fiber. The vertical bars in equation 36, denote absolute value, which is essential to ensure that the expression yields β and not the supplementary angle. This is a minor point that has not been addressed in literature but is worth mention due to considerable confusion that it can cause when calculating TCA angle or actuation. Radial swelling of a circular cross-section causes an increase in $I = \frac{\pi R^4}{4}$ and $J = \frac{\pi R^4}{2}$, and thus a change in β. For circular cross-section, Equation 36 can be expressed in more compact form to see that $cos\beta$ depends on the square of the fiber radius, R.

$$cos\beta = \left| \frac{nR^2 \sqrt{\frac{\pi E}{\mathbf{F}}} - \frac{E}{G} - 2}{\frac{E}{G} - 2} \right| \quad (37a)$$

Based on the presence of n, $cos\beta$ is also inversely related to fiber length, l_a. Note that for an ideal elastomer, $E = 3G$, and equation 37a can be further simplified.

$$cos\beta = \left| nR^2 \sqrt{\frac{\pi E}{\mathbf{F}}} - 5 \right| \quad (37b)$$

Since $nR^2 \sqrt{\frac{\pi E}{\mathbf{F}}}$ must be less than 5, as R increases, $cos\beta$ decreases; in other words β increases with fiber swelling, as required for coil contraction. Knowing $cos\beta$, the strain of the coil is

$$\varepsilon = \frac{\Delta L}{L_i} = \frac{l_{a,f}cos\beta_f}{l_{a,i}cos\beta_i} - 1. \quad (38)$$

Refer to Supporting Information for derivation of Equation 38. The two limits of actuation occur when $\frac{\Delta l_a}{l_a} = 0$ and $\frac{\Delta l_a}{l_a} = \frac{\Delta R}{R}$. A perfectly anisotropic material in which swelling only occurs in the radial direction $\left(\frac{\Delta l_a}{l_a} = 0 \right)$ will achieve maximum stroke because axial contraction due to TCA effects is not offset by material swelling in the axial direction. Minimum possible TCA stroke will occur in an isotropic material that swells equally in all directions $\left(\frac{\Delta l_a}{l_a} = \frac{\Delta R}{R} \right)$. The magnitude of the minimum axial stroke of a coiled fiber will be at least double the linear (uncoiled) swelling, and more typically an order of magnitude greater for practically achievable coil geometries. For radial swelling of homochiral coils, $cos\beta_f < cos\beta_i$. Thus, equation 38 indicates that a homochiral coil will contract due to radial swelling. Equation 38 also accounts for axial swelling, which slightly reduces actuation because the swollen fiber length, $l_{a,f}$, is greater than the initial fiber length, $l_{a,i}$.

An experimenter, after loading the artificial muscle with a known force and knowing the mechanical properties of the polymer material used to make the artificial muscle, may use equation

(38) to determine the coil bias angle, as long as a sufficient amount of twist is inserted to cause the fiber to coil. The critical amount of twist needed to induce coiling is also predicted by elastic rod theory.[53] Moreover, the actuation of said coil can be determined from equations 37 and 38 based on radial swelling (and axial swelling if it occurs).[31, 53] In reality, coil contraction ceases when adjacent coils come into contact. This condition occurs when the fiber diameter exceeds the coil pitch.

$$2R \geq p = \frac{l_a cos\beta}{N} \quad (39)$$

N is the number of coils, which, following Lamuta, et al., is a function of bending stiffness, EI, and applied load.

$$N = \frac{l_a}{2\pi}\sqrt{\frac{\mathbf{F}}{EI}} \quad (40)$$

As the fiber swells and the coil contracts, this condition must be considered to ensure that calculated coil strains are physically possible.

2. Work done

The work done by a TCA will depend on the applied load. The load applied in the form of tensile stress elongates the coil which in turn provides room for contraction during actuation. This load can be the same or different as that used to form the coil.[31, 32, 54, 55] The work per coil length can be calculated simply by $\frac{W}{L} = F\frac{\Delta L}{L}$. Thus, the output of the 1D radial transport/swelling model can be fed into the analytical TCA expressions to determine dynamic actuation and transient work.

Results

The effect of polymer-solvent combination (i.e. χ) on equilibrium swelling has been examined over a wide range of solvent quality. The dependence of volume ratio on χ is shown in Figure 1(a). This comes from the implicit solution of Equation 11. Negative values of χ correspond to attractive interaction between solvent and polymer that results in a large amount of swelling. As the solvent quality becomes poorer (χ increases), the amount of swelling is less. In the limit of a poor solvent ($\chi > 0.5$), very little solvent enters the polymer and volume ratio asymptotically approaches the dry value of 1. Interaction parameters for a variety of polymer-solvent combinations can be found in the *Polymer Handbook*.[56]
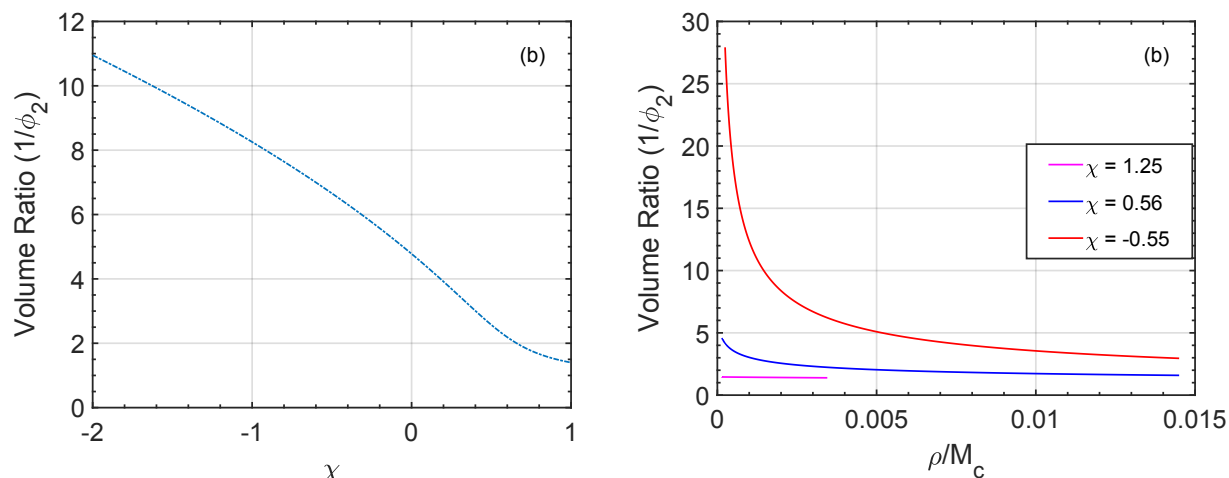
Figure 1. When fixed, $M_n = 200{,}000$ g/mol, $M_c = 1000$ g/mol, $\chi = 0.56$, $v_1 = 18$ cm^3/g, $\rho = 1.45$ g/cm^3 **(a)** Equilibrium swelling increases with increasing solvent quality (more negative χ). M_c, M_n, ρ, and v_1 are fixed. **(b)** Equilibrium swelling decreases with increasing crosslink density $\rho/(M_c)$. M_n, ρ, and v_1 are fixed. The values of χ shown in the legend are also fixed for each data set. Volume ratio refers to equilibrium values after complete swelling.

Once a polymer-solvent combination is chosen, the modulus of the material and the degree of swelling can be tuned via the degree of crosslinking. The relationship between the crosslink density, $1/(\bar{v} M_c)$, and volume ratio is shown in Figure 1(b). In this case, the value of χ is fixed and equilibrium polymer volume fraction is solved for different crosslink densities. This is a parameter that is used in the tuning of the fiber strength and durability. Crosslink density can be controlled using a range of techniques that are applicable to forming muscle fibers.[57, 58] As the density of crosslinks increase, the length of segments between crosslinks decrease. With fewer segment configurations to explore, the penalty for stretching becomes greater, which means that the elastic component of the Gibb's free energy change is larger. Thus, the polymer swells less (as shown) and the plateau modulus of the polymer increases. Note that as crosslink density approaches zero, the volume ratio tends to infinity, as is expected for dissolution of an uncrosslinked polymer. Similar to large χ, for sufficiently large crosslink density, the volume ratio is expected to tend to 1.

The equilibrium swelling condition from the thermodynamic calculation is enforced in the transport model via the boundary condition on the outside of the fiber, which is the maximum x or r value for Cartesian or cylindrical coordinates, respectively. As described in the methods section, the swelling of each differential element is dictated by the local, transient solvent volume fraction. This swelling process increases the distance for diffusion over time as the control volume swells first near the outer boundary and eventually throughout as the solvent penetrates into the center of the control volume. Thus, swelling slows diffusion and gradually increases the outer boundary position of the fiber, R. An example of this diffusion process is shown in Figure 2(a) for Cartesian coordinates with $\chi = 0.56$, $D = 1 \times 10^{-5}$ mm^{2}s^{-1}, $X_i = 0.1$ mm, $\nabla \Phi = 0$ V. Transient concentration profiles are shown. At time zero, there is a step change at the outer boundary ($x = 0.1$ mm) from a dry slab ($C = 0$) to the equilibrium condition ($C = 0.64$). As time proceeds,

the solvent diffuses into the slab, eventually reaching $x = 0$, after which the concentration continues to increase toward the equilibrium condition. As the solvent concentration increases, the outer boundary of the slab, X, increases. In other words, X is a function of time. This can be seen more clearly in the magnified view in Figure 2(b). The outer slab position can be directly calculated simply by summing all the differential step sizes. Swelling occurs immediately at the outer boundary and proceeds in increasing fashion as elements deeper in the slab are swollen and outer elements are swollen further.
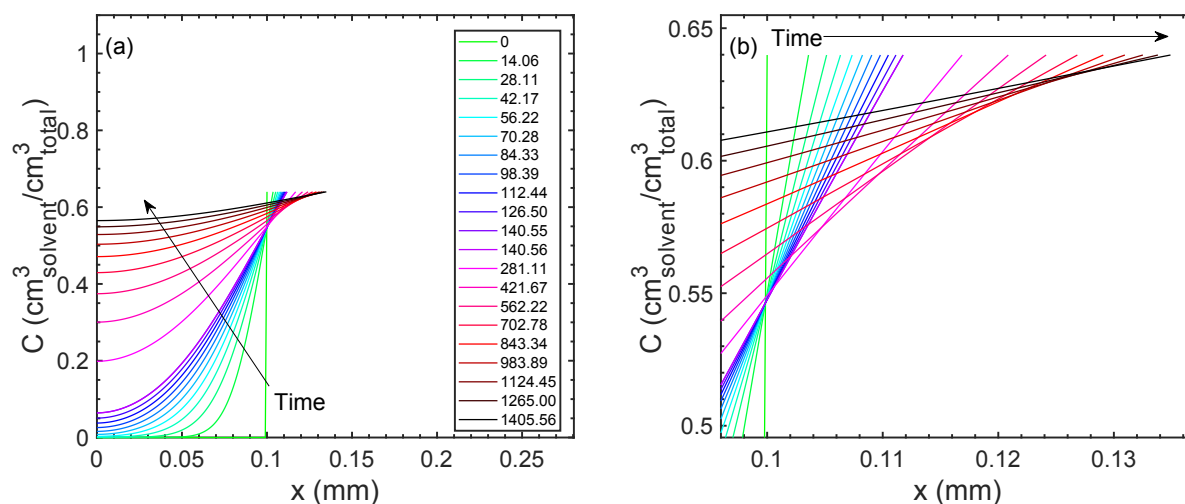

Figure 1. (a) Concentration profile in a polymer sample of 0.1 mm initial thickness. Concentration profiles of solvent volume fraction are captured at a range of times shown in the legend in seconds. **(b)** Zoomed section of concentration profile showing the swelling of the outer boundary with time. For both figures, $M_n = 200{,}000$ g/mol, $M_c = 1000$ g/mol, $\chi = 0.56$, $v_1 = 18$ cm^3/g, $\rho = 1.45$ g/cm^3, $D = 1 \times 10^{-7} \frac{\text{cm}^2}{\text{s}}$, and $T = 298\ K$.
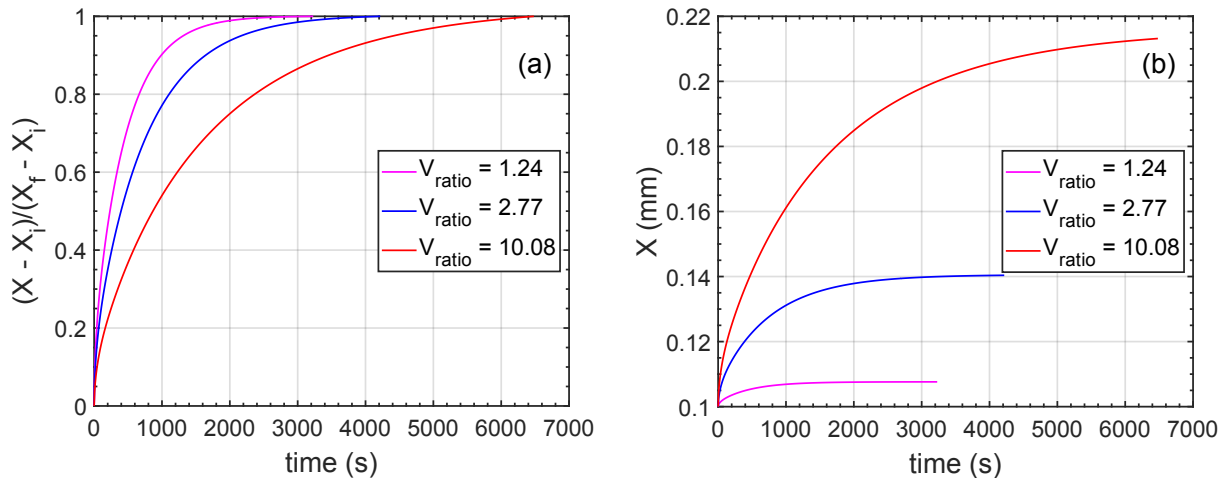
This is a significant development in that the model is able to predict the transient volume change due to the solvent concentration change, $C = 1 - \phi_2$, that has occurred over time. Figure S1 shows the concentration profile after complete swelling. To ensure near complete swelling occurs, the final time is run to 3 times the characteristic diffusion time, t_d, and is calculated using the volume

ratio of a fully swollen polymer-solvent system, where for a fiber it is

$$Time_{final} = 3 * t_d = 3 * \frac{\left((\phi_2)^{-1/3}R_i - R_{ii}\right)^2}{D}. \qquad (41)$$

The final outer radius, $R_f = (\phi_2)^{-1/3}R_i = V_{ratio}^{1/3}R_i$, is related to the initial outer radius and the equilibrium V_{ratio}. An initial inner radius, R_{ii}, can also be included if the fiber contains an electrode or other nonswellable component. For the slab of Figure 2, $R_i = X_i$ and $R_{ii} = 0$.

The amount of swelling at equilibrium, embodied by the thermodynamically determined volume ratio, affects the time to equilibrium. This is depicted in Figure 3(a), where the only difference among the 3 curves is V_{ratio} that was varied by changing the polymer-solvent interaction parameter. The outer position of the control volume, X, is normalized by the initial and final positions in Figure 3(a). No electromotive force is applied in these calculations. All 3 simulations in Figure 3(a) have the same initial dimensions. The difference is the amount of swelling that occurs. Clearly, the transient increase in diffusion distance due to swelling, as seen in Figure 3(b), causes a large increase in the time to equilibrium. The time to reach 90% of final swelling, $t_{90\%}$, is used to quantitatively compare the 3 simulations and is shown in Table 4 along with the equilibrium solvent volume fraction for each volume ratio. The characteristic diffusion time without any swelling is $t_{d,i} = X_i^2/D = 1,000$ s, which is not a function of equilibrium solvent concentration. With swelling, t_d is a function of the equilibrium solvent concentration as shown in Equation 41. Only 90% of equilibrium is achieved in $t_{d,i}$ for $\phi_1 = 0.19$. With increased swelling, $t_{90\%}$ increases with $V_{ratio}^{2/3}$, as expected based on Equation 41. Figure 3(b) shows the non-normalized swelling of a fiber by plotting the outer radius values versus time. Given a larger volume ratio with all other parameters equal, a fiber takes longer to fully swell, and at $V_{ratio} = 10$, the outer radius size doubles.
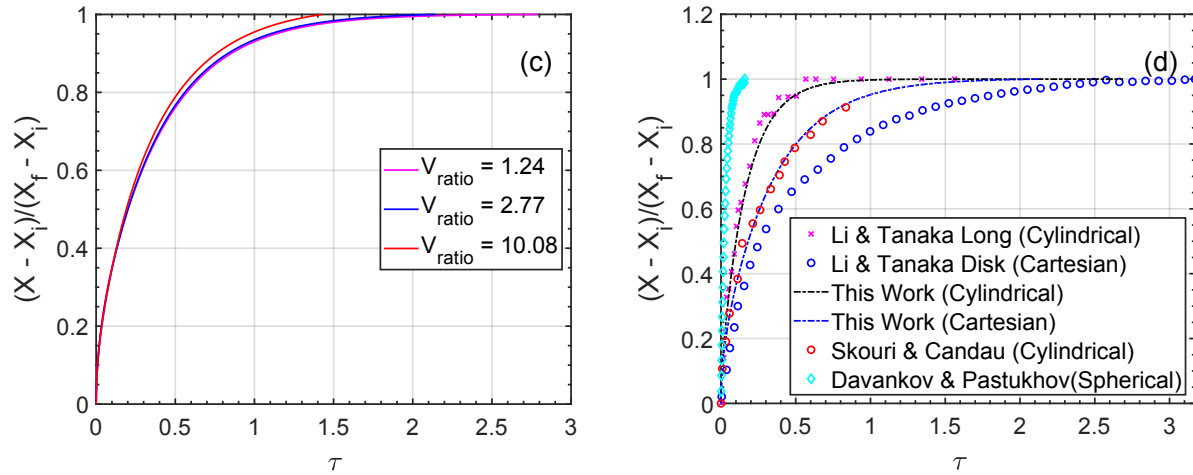
Soft Matter Accepted Manuscript

Figure 3. (a) Effect of polymer and solvent characteristics on transient, normalized slab size. **(b)** Magnitude of outer slab growth over time. **(c)** Normalized slab thickness with respect to dimensionless time, $\tau = \frac{t}{t_d}$. **(d)** $X = R$. Comparison of this model with moderately crosslinked PAA cylinders from Skouri and Candau, 1995[60, 63], Li and Tanaka's acrylamide cylinder and disk gels [61], and Davankov and Pastukhov's[62] spheres of polystyrene in water vapor. For this work, $V_{ratio} = 1.24$, $\chi = 1.25$; for $V_{ratio} = 2.77$, $\chi = 0.56$; for $V_{ratio} = 10.08$, $\chi = -0.55$. For all figures, $M_n = 200{,}000$ g/mol, $M_c = 1{,}000$ g/mol, $v_1 = 18$ cm^3/g, $\rho = 1.45$ g/cm^3, $D = 1 \times 10^{-7} \frac{cm^2}{s}$, $T = 298\ K$, and $\nabla\Phi = 0$ V/mm.

Table 4. Time to reach 90% of equilibrium swelling for pure diffusion in Cartesian coordinates. For all rows, $M_n = 200{,}000$ g/mol, $M_c = 1{,}000$ g/mol, $v_1 = 18$ cm^3/g, and $\rho = 1.45$ g/cm^3, $D = 1 \times 10^{-7} \frac{cm^2}{s}$, $T = 298\ K$, and $X_i = 0.1$ mm.

V_{ratio}	$\nabla\Phi$ (V/mm)	$t_{90\%}$ (s)	χ	ϕ_1	Figure
1.24	0	993	1.25	0.19	3
2.77	0	1,673	0.56	0.64	3, 4
	0.123	1,469			4
	1.23	620			4
	12.3	55			4
10.08	0	3,456	-0.55	0.90	3

Figure 3(c) is a display of the fully non-dimensionalized fiber growth versus their respective non-dimensional time, τ. The simulations with different volume ratios have non-dimensionalized results that nearly perfectly collapse onto one another except for the highest volume ratio, 10.08, which was not run to $3t_d$ due to computation time limitations. Even still, the largest volume ratio simulation has similar behavior to the other volume ratio simulations, which is clearly demonstrated in the non-dimensionalized form presented in Figure 3(c).

All these results are based on a constant diffusion coefficient. The change in magnitude of concentration from the dry to the swollen state is quite significant for larger swelling ratios, such as a value of 10. In this case, the diffusion coefficient could exhibit concentration dependence that is not captured in the current model. It has been reported that deviation from Fickian behavior is consistent with studies by Crank [59] and discussed by Neogi [10] due to the dependence of diffusivity on concentration change. In such cases, an average value of the diffusion coefficient over the concentration range has been shown to accurately describe sorption of solvent into polymers. Our numerical model tracks the local concentration in each differential element, and could therefore be adjusted to incorporate diffusion coefficients that are functions of the calculated concentration in future work. The remainder of this work focuses on $V_{ratio} = 2.77$, a value at which concentration dependence of diffusion coefficient is expected to be much less significant. In fact, the diffusion coefficient used in the model is based on water in Nafion, which has been shown to have no significant concentration dependence.[44]

A comparison of our results to experimental data is made in Figure 3(d) using Skouri, et al.[60], Li and Tanaka [61], and Davankov and Pastukhov [62]. These data were chosen based on their reporting absolute dimensions and volumetric swelling of polymeric networks by solvent (in all cases water). The data from Skouri, et al. is for dry polyacrylic acid (PAA) swollen with 0.117 NaCl aqueous solution. One of a set of polyelectrolyte gels of PAA of varied ionic strengths prepared by Skouri, et al. was chosen for comparison here. The particular PAA sample reported here has a final diameter of 8.4 mm and a molar concentration ratio of bisacrylamide to acrylic acid units of 0.02, i.e. the degree of polymerization of a crosslink strand is approximately 100, from which the crosslink density can be estimated. Li and Tanaka used acrylamide gels of standard composition (5 g of acrylamide and 0.133 g of bisacrylamide) prepared by free radical polymerization. They report swelling data for acrylamide gels of a variety of cylindrical proportions, i.e. disk, short cylinder, long cylinder and very long cylinder. The long cylinder was compared to our cylindrical model, and the disk was compared to our Cartesian model. The initial radius for the long cylinder is 0.675 mm, and the final radius is 0.75 mm. The final thickness of the disk is 1.47 mm based on an initial thickness of 1.33 mm. Davankov and Pastukhov report 74% volumetric swelling of 0.6 to 0.8 mm diameter polystyrene spheres in water.

Since all the necessary parameters for the model are not available, the model and literature data are compared in dimensionless form in Figure 3(d). Table 5 contains the key values necessary to generate Figure 3(d) from dimensional data reported in the references. The Cartesian model of this work approaches equilibrium more rapidly than does the disk swelling data of Li and Tanaka and actually coincides with the fiber measurements of Skouri, et al. They conclude that electric charges affect the elasticity of the samples and thereby the swelling results, which could explain the apparent discrepancy. In addition to the Cartesian model result, a curve is shown from this work for cylindrical coordinates, which actually agrees well with the long fiber of Li and Tanaka. It is clear from both the literature data and the model results that transport rate is faster in curved coordinates. In fact, the results of Davankov and Pastukhov for spheres has the most rapid approach to equilibrium, which indicates that transport rate is a function of the degree of symmetry. This is a rather well-known effect that is due to the dependence of flux cross-sectional area on the radial position in the control volume. Future work with and without charged networks will be conducted in order to better understand the lack of complete agreement between the model developed in this work and experimental measurements. However, it is worth pointing out that the

disagreement between our Cartesian model and the disk of Li and Tanaka is no greater than the disagreement between the two experimental results for cylindrical fibers.

Table 5. Samples from literature compared to this work in Figure 3d from Li & Tanaka, Skouri & Candau, and Davankov.

Geometry	Combination	V_{ratio}	D $(cm^2 s^{-1})$	t_d (s)	Reference
Cylinder	PAA-Water	17.64	3.5×10^{-6}	5×10^4	[60]
Disk	PAM-Water	1.35	2.9×10^{-7}	2×10^4	[61]
Cylinder	PAM-Water	1.37	2.9×10^{-7}	2×10^4	
Sphere	PS-Water Vapor	5.32	1×10^{-7}	4×10^4	[62]

Figure 4 shows the normalized growth of a sample slab with time, with and without applied potential. In the simulations with applied potential, electrodes on either side of the slab induce a gradient of electric potential (voltage) across the sample. This electric potential is the source of migration of solvent/ions from one electrode toward the other. At an EMF of 1.23 V/mm, 90% of equilibrium swelling is achieved in 620 s as opposed to 1673 s without an applied potential. The magnitude of the voltage gradient was varied while maintaining all other parameters constant, which caused a pronounced increase in growth rate with increasing voltage gradient. The maximum voltage for an aqueous system results in a maximum gradient of 12.3 V/mm for the 0.1 mm thick slab used in this simulation. An EMF of 12.3 V/mm exhibited swelling to 90% of equilibrium in just 55 s. Thus, the slowing down of diffusion due to swelling can be more than compensated by applying an electric field. Interestingly, at low applied potential (e.g. 0.123 V/mm), there are diminishing enhancements to the actuation rate. The time to 90% swelling for each simulation is shown in Figure 4 and reported in Table 4.
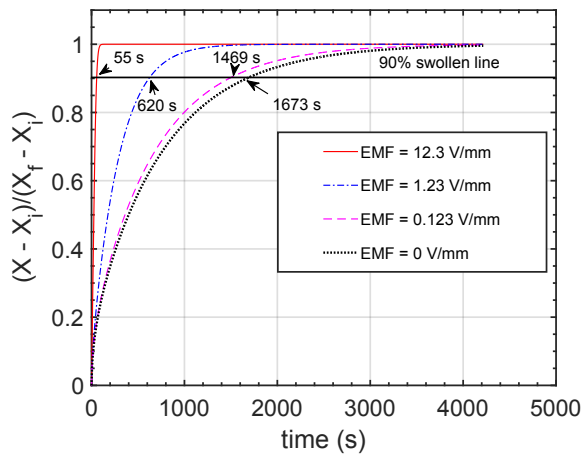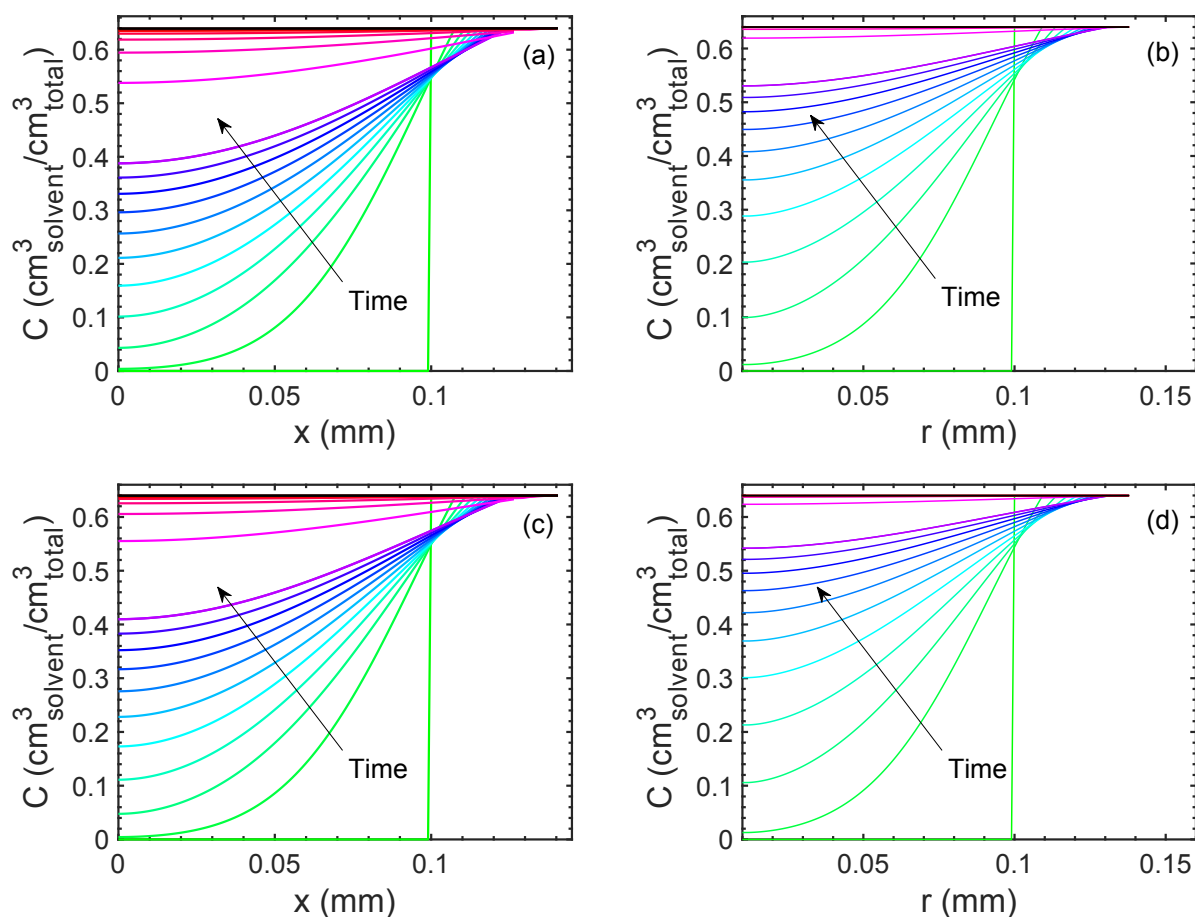

Figure 4. Effect of magnitude of EMF on swelling rate. $M_n = 200,000$ g/mol, $M_c = 1000$ g/mol, $\chi = 0.56$, $V_{ratio} = 2.77$, $v_1 = 18$ cm^3/g, $\rho = 1.45$ g/cm^3, $D = 1 \times 10^{-7} \frac{cm^2}{s}$, $T = 298$ K, and X_i

$= 0.1$ mm.

In comparing the two geometries and how EMF affected both, Figure 5 was generated with all variables being equal, except R_{ii} that was set to a small non-zero value in cylindrical coordinates in order to allow for the presence of an inner electrode. In Cartesian coordinates, Figures 5 (a), (c), and (e) progressively show that a positive EMF increases the flux into the polymer sample. The final profiles (black lines) show that the equilibrium concentration is achieved regardless of the magnitude of applied potential. In cylindrical coordinates without EMF, Figure 5 (b) shows that the equilibrium concentration is also achieved. Figures 5 (b), (d), and (f) demonstrate that a positive EMF increases the flux in cylindrical coordinates as well. Figures 3(d) and 5 show that the cylindrical model reaches equilibrium more rapidly than does the Cartesian model, as discussed above.
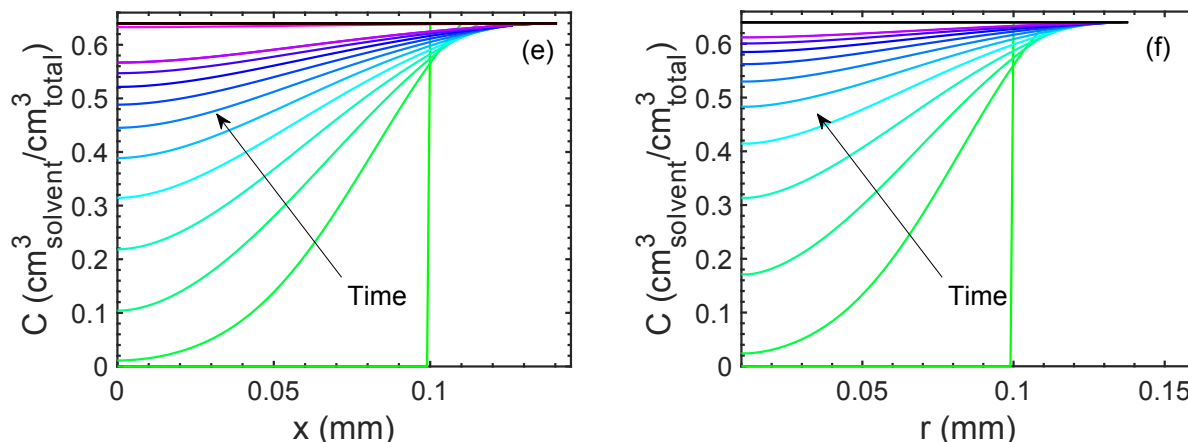
Figure 5. Comparison of Cartesian to cylindrical numerical calculations. Figures (a), (c), and (e) are results in Cartesian coordinates at **(a)** 0 V/mm, **(c)** 0.123 V/mm and **(e)** 1.23 V/mm. Figures (b), (d), and (f) are results in cylindrical coordinates at **(b)** 0 V/mm, **(d)** 0.123 V/mm and **(f)** 1.23 V/mm. For all Cartesian figures, initial time increments are 51 seconds, and for profiles of count 10 and higher, 511 seconds is the increment in time. For cylindrical, initial time increment is 59 seconds and 592 seconds for later times. For both coordinate systems, Cartesian and cylindrical, M_n = 200,000 g/mol, M_c = 1000 g/mol, χ = 0.56, v_1 = 18 cm^3/g, ρ = 1.45 g/cm^3, D = 1 × 10^{-7} $\frac{cm^2}{s}$, T = 298 K, $X_i = R_i$ = 0.1 mm. Final times are 5113 s and 5927 s for Cartesian and cylindrical coordinates, respectively. To allow for an inner electrode, the simulation in cylindrical coordinates has a non-zero inner radius, R_{ii} = 0.01 mm.

Finally, a negative voltage gradient was used to examine the case when migration flux is in the opposite direction of diffusive flux. Results are shown in Figures 6(a) and (b). In both Cartesian and cylindrical coordinates, a reduction in the swelling rate was observed, such that thermodynamically calculated equilibrium swelling was not achieved within the total simulation time for the Cartesian coordinate system. In the cylindrical coordinate system, a steady-state concentration profile appears to be achieved but the rate of swelling to an equilibrium state is slower than that for a positive potential gradient. Thus, the negative migration term results in slower swelling. Figure 6(c) is a comparison of fiber growth with no EMF and a negative EMF (-1.23 V/mm) for the cylindrical version. This result confirms that migration can be used to modulate concentration and swelling rate within shorter-than-equilibrium times, yielding a preliminary prediction that rapid, controllable actuation can be achieved with electric fields, especially if coupled with changing boundary conditions.
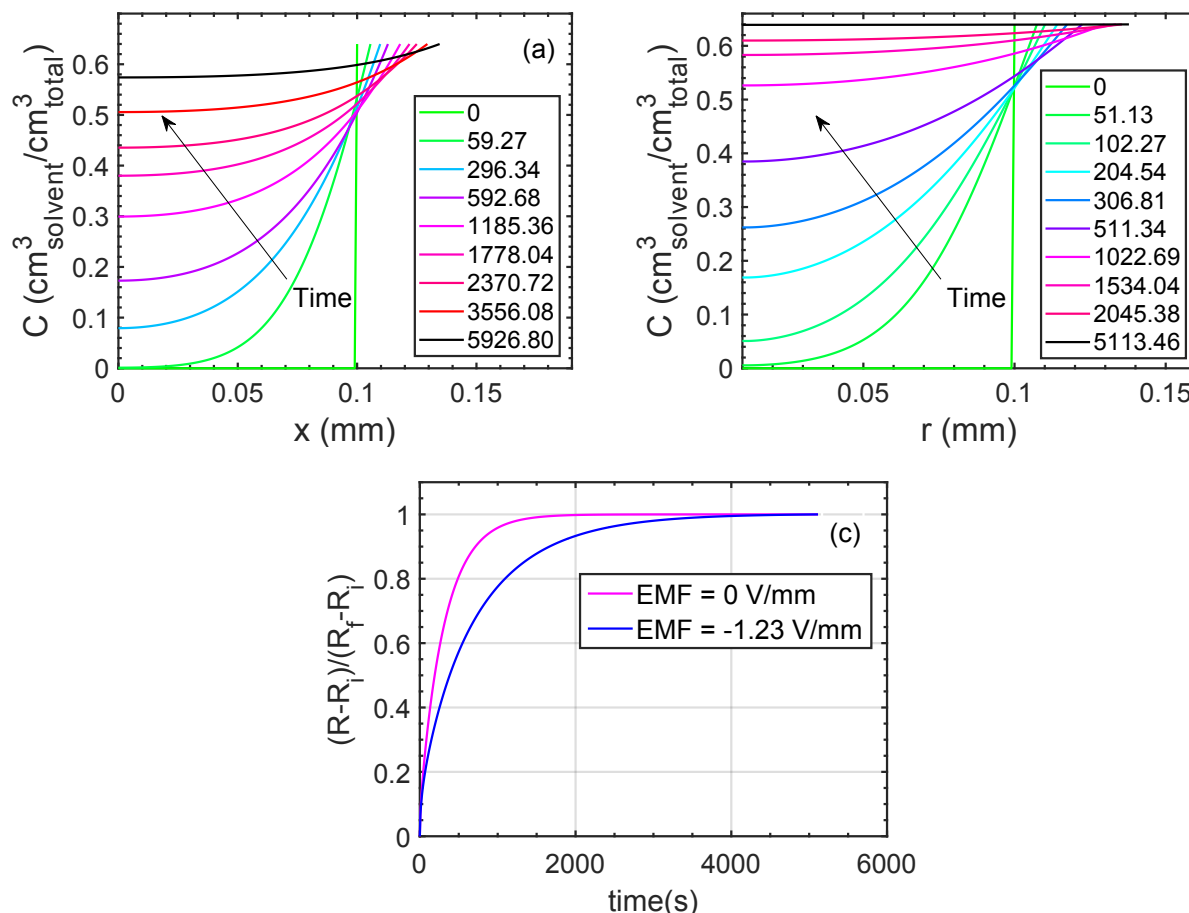
Figure 6. Effect of a negative voltage across a polymer sample (EMF $= -1.23$ V/mm) in **(a)** Cartesian and **(b)** cylindrical coordinates. Time of each profile in seconds is denoted in the legend. **(c)** Comparison of a fiber with no EMF to a fiber influenced by a negative EMF of -1.23 V/mm in cylindrical coordinates. For **(a)**, **(b)**, and **(c)**, $M_n = 200{,}000$ g/mol, $M_c = 1000$ g/mol, $\chi = 0.56$, $v = 18$ cm^3/g, $\rho = 1.45$ g/cm^3, $X_i = R_i = 0.1$ mm. For **(a)**, $R_{ii} = 0$ mm. For **(b)** and **(c)**, $R_{ii} = 0.01$ mm.

Discussion

An assumption inherent in the current model is that polymer relaxation is not rate limiting such that the polymer in each differential element can instantaneously swell in response to transient changes in concentration due to diffusion and migration. This assumption is reasonable for rubbery polymers, which is the intended application of the model. This assumption would not be appropriate for glassy materials, in which swelling does not occur unless the solvent causes plasticization. This can also be a concern in thin films where confinement can have a large effect on glass transition temperature. This is highlighted by the fact that Nafion relaxation due to water sorption is not rate limiting in the bulk,[44] but is rate limiting in Nafion thin films.[65] Thus, the current model is appropriate for swelling of bulk, rubbery networks, but would need to be modified to account for polymer relaxation in glassy materials and thin films.

As a proof of concept that this model can be used to evaluate TCA actuation, a hypothetical coil

was constructed by inserting 3979 turns into a 1-meter-long fiber with 30 N of tensile force applied. The fiber has a Young's modulus of 2.5 GPa and a shear modulus of 0.83 GPa. The resulting coil is rather loose, with a bias angle, β, of 17° that provides room for radial swelling and concomitant axial contraction. Figure S2 schematic is provided for proper definition and visualization of β. Although coil performance can be optimized by using a greater load during actuation than that used during coil formation,[32] for simplicity the same load of 30 N was maintained during actuation in this work. The swelling data from Figure 4 was used to determine the outer radius of the fiber as a function of time, and equations 37 and 38 were used to determine theoretical axial strain.[31] The condition of coil-coil contact (equation 39) was used to determine when axial contraction of the coil would cease. Figure 7(a) shows coil contraction as a function of time up to the point when adjacent coils come into contact. As shown in Figure 7(a), rapid contraction of the coil occurs when significant EMF is applied. Figure 7(a) has a second horizontal axis which shows the dependence of coil strain on the volume ratio for the smallest electric field (0.123 V/mm). It also makes clear the relationship between volume ratio and time for that data set. The simple cubic relationship between fiber radius and volume ratio is shown in Figure S3(a) and the relationship between coil strain and volume ratio is shown more directly for all 3 data sets in Figure S3(b). It demonstrates that the electric field does not affect the amount of swelling, but only the rate of swelling. It also shows that for the parameters used in this study and over the range of swelling examined the coil strain has an approximately linear response to volumetric swelling.

Figure 7(a) is for the case of a perfectly anisotropic fiber that only swells radially and not along the fiber length. As shown in Figure S4(a), an isotropic material still maintains benefits of coiling, but would exhibit equilibrium axial strain of -0.794, as compared to -0.811 for the anisotropic fiber. Finally, the work done is also calculated as the product of the change in coil length and the load. As shown in Figure 7(b), upon full contraction the anisotropic case does 23.2 J of work, whereas the isotropic case would do 22.7 J of work against a 30 N load. Clearly, the initial power (early time slope in Figure 7(b)) increases significantly with EMF.

As mentioned above, as the volume ratio increases the coil strains negatively (contracting in length). This is the absolute upper limit on possible coil strain for the chosen parameters. It could only be achieved if a perfectly anisotropic material with constant modulus were used to construct the fiber so that it swells only in the radial direction and not in the length direction. This might be possible with a composite or if a solid electrode core were present in the center of the fiber, as has been considered in this work. An isotropic material that swells equally in curvilinear length of the fiber as it does in the radial direction would exhibit a final coil strain that is reduced by a factor of $V_{ratio}^{1/3} - 1$. The coil strain reported in Figure 7(a) is also only possible if swelling of the material has no impact on the shear modulus. Scaling laws can be used to estimate the possible impact of swelling on network modulus.[66] Based on the chi parameter used in this modeling case, the solvent can be considered athermal for the network, which is the limiting case of a good solvent. In this limit, the shear modulus decreases with increasing volume ratio in a power law fashion, $E = 3G \sim V_{ratio}^{-0.56}$. Since the network is considered ideal, both tensile and shear modulus exhibit the same dependence on V_{ratio}. For this case, the final $V_{ratio} = 2.77$, and G is reduced to 4.7×10^8 Pa and E is reduced to 1.4×10^9 Pa. As outlined in the supporting information, the network modulus is proportional to polymer density. The most extreme possible situation would entail modulus scaling inversely with V_{ratio}. As shown in Figure S4(b), this has a dramatic effect on coil strain, decreasing it from -0.811 for a material with constant modulus to -0.183. This nearly order of

magnitude reduction of coil strain emphasizes the importance of using an inner core that maintains approximately constant modulus and an outer shell that swells to increase radius, as has been done with sheath-run artificial muscles.[33, 67, 68] Composites might be an alternative artificial muscle design approach to maintain nearly constant moduli and anisotropic swelling.
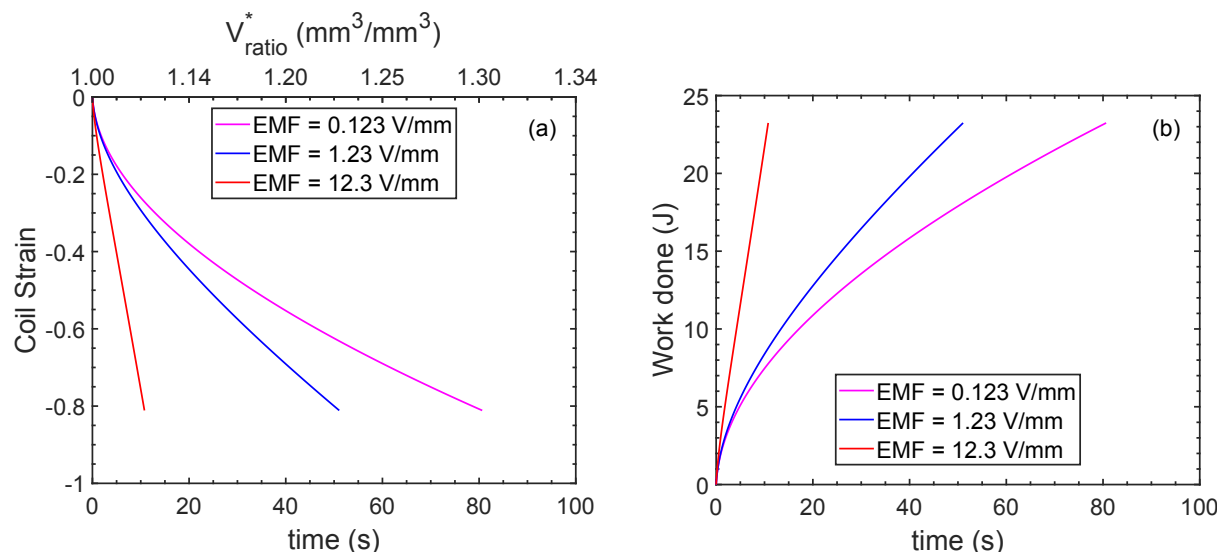

Figure 7. (a) Coil strain due to radial swelling over time (taken from Figure 4) as a function of time. *Second horizontal axis applies only to EMF = 0.123 V/mm. **(b)** Work done by coil contraction; rate is enhanced by increased electromotive force (V/mm) in a TCA fiber under $F = 30$ N of load. $G = 8.3 \times 10^9$ Pa, $n = 25,000$ rad/m, $E = 2.5 \times 10^9$ Pa, $R_i = 0.1$ mm, and $l_a = 1,000$ mm.

Conclusions

Swelling of polymer fibers and slabs was modeled numerically and parametric studies conducted. This study will aid efforts to identify the best material candidates for practical use as artificial muscle fibers. Unlike empirical approaches that are limited by available chemistry, the approach taken in this study begins with first principles and seeks to predict the actuation behavior of polymer-solvent combinations for which the interaction parameter is known. The polymer with the poorest solvent was able to achieve the 5% strain target, suggesting that dynamics is the greater challenge. The modular design of the code allows for boundary conditions to be changed to Neumann, Robin or Dirichlet.[39] Initial conditions are changeable and charge-containing polymers can be studied if diffusion and migration play a role in actuation. This model can be adjusted to handle other materials and actuation mechanisms. For example, the model could be readily adapted to handle thermal diffusion. Fiber radius changes more quickly with the introduction of a voltage, which is essential to meet targets based on natural muscles. In fact, this work indicates that, in addition to migration, smaller dimensions than those used here are needed to achieve the sub-second response times of natural muscles. Introduction of voltage translates to an increase in power that can be done by a polymer-solvent system used as a twisted and coiled artificial muscle. In the comparison of a cylindrical fiber from literature, experimental data agrees well with this model. This study has shown that the code produced can predict actuation of a TCA

artificial muscle given χ, M_n, M_c, specific volume of the solvent, density of the polymer, voltage applied, diameter, length of fiber before twisting, Poisson's ratio, Young's Modulus, amount of inserted twist, and the load applied to the fiber.

Conflicts of interest
There are no conflicts to declare.

Acknowledgments

Nomenclature

α_s: linear deformation factor ($\frac{R}{R_i}$)

β: Coil bias angle

C: Solvent concentration (volume fraction)

d: Coil diameter (mm)

D: Diffusion coefficient (mm^2/s)

$\mathbf{E}$: Electric field (V/mm)

E: Elastic modulus (Pa)

$\mathbf{F}$: Applied load (N)

$\mathcal{F}$: Faraday's constant (C/mol)

G: Shear modulus (Pa)

ΔG_{sw}: Gibbs free energy of swelling the polymer network (J/mol)

ΔG_{mix}: Gibbs free energy change due to mixing (J/mol)

ΔG_{el}: Gibbs free energy change due to stretching of elastically active network chains (J/mol)

Φ: Electric potential (V)

ϕ_1: Solvent volume fraction, $\frac{V_{solvent}}{V_{swollen\ polymer}}$

ϕ_2: Polymer volume fraction $\frac{V_{dry\ polymer}}{V_{swollen\ polymer}}$

k: Boltzmann's constant (J/K)

L: Unloaded coil length (mm)

l_a: Fiber length (mm)

$n = \Delta\tau/l_a$: Inserted twist (in radians) per fiber length (rad/mm)

N_1: Number of solvent molecules

N_2: Number of polymer molecules

N_A: Avogadro's number (mol^{-1})

N_{bc}: Number of crosslinks per mole of chains

N_i: Flux (mol mm^{-2} s^{-1})

M_c: Molecular weight between crosslinks (g/mol)

M_n: Uncrosslinked polymer molecular weight (g/mol)

R: Fiber radius (mm)

R_i: Initial fiber radius (mm)

R_{ii}: Inner fiber radius (mm)

R_f: Final fiber radius (mm)

R_{gas}: Gas constant (J mol^{-1} K^{-1})

t: Time (s)

t_d: Characteristic diffusion time (s)

T: Temperature (K)

ΔU: Change in number of turns of a fiber

u_i: Mobility (mm^2 mol J^{-1} s^{-1})

μ_s: Chemical potential of the solvent within the swollen polymer

μ_s^0: Chemical potential of the pure solvent

$\bar{v} = \frac{1}{\rho}$: Specific volume of polymer (mm^3/g)

v_1: Molar volume of solvent (mm^3/mol)

v_2: Molar volume of polymer (mm^3/mol)

V_{ratio}: Ratio of swollen polymer volume to dry polymer volume, $\frac{1}{\phi_2} = \frac{V_{swollen\ polymer}}{V_{dry\ polymer}}$

W: Work (J)

x, r: Position (mm)

X, R: Outer position of slab (mm), Outer position of fiber (mm)

χ: Flory-Huggins polymer-solvent interaction parameter

z_i: Charge number

Soft Matter Accepted Manuscript

References

[1]   N. A. Atikah, L. Y. Weng, A. Anuar, C. C. Fat, I. Z. Abidin, and K. S. M. Sahari, "Development of nylon-based artificial muscles for the usage in robotic prosthetic limb," *AIP Conference Proceedings,* vol. 1883, no. 1, p. 020042, 2017, doi: 10.1063/1.5002060.

[2]   M. Kanik *et al.*, "Strain-programmable fiber-based artificial muscle," *Science,* vol. 365, no. 6449, pp. 145-150, 2019, doi: 10.1126/science.aaw2502.

[3]   J. S. Hyeon, J. W. Park, R. H. Baughman, and S. J. Kim, "Electrochemical graphene/carbon nanotube yarn artificial muscles," *Sensors and Actuators B-Chemical,* vol. 286, pp. 237-242, May 2019, doi: 10.1016/j.snb.2019.01.140.

[4]   Y. Tadesse, A. Villanueva, C. Haines, D. Novitski, R. Baughman, and S. Priya, "Hydrogen-fuel-powered bell segments of biomimetic jellyfish," *Smart Materials and Structures,* vol. 21, no. 4, p. 045013, 2012/03/20 2012, doi: 10.1088/0964-1726/21/4/045013.

[5]   K. J. Kim *et al.*, "Enhancing the Work Capacity of Electrochemical Artificial Muscles by Coiling Plies of Twist-Released Carbon Nanotube Yarns," *Acs Applied Materials & Interfaces,* vol. 11, no. 14, pp. 13533-13537, Apr 2019, doi: 10.1021/acsami.8b21417.

[6]   H. Okuzaki, H. Suzuki, and T. Ito, "Electrically driven PEDOT/PSS actuators," *Synthetic Metals,* vol. 159, no. 21, pp. 2233-2236, 2009/11/01/ 2009, doi: https://doi.org/10.1016/j.synthmet.2009.07.054.

[7]   K. Peters, J. Braun, B. Schmidt-Hansberg, P. Scharfer, and W. Schabel, "Phase equilibrium of water in different types of PEDOT:PSS," *Chemical Engineering and Processing: Process Intensification,* vol. 50, no. 5, pp. 555-557, 2011/05/01/ 2011, doi: https://doi.org/10.1016/j.cep.2010.11.005.

[8]   T. Mirfakhrai, J. D. W. Madden, and R. H. Baughman, "Polymer artificial muscles," *Mater. Today,* vol. 10, p. 30, 2007.

[9]   M. Amjadi and M. Sitti, "High-performance multiresponsive paper actuators," *ACS nano,* vol. 10, no. 11, pp. 10202-10210, 2016.

[10]   P. Neogi, *Diffusion in polymers* (Plastics engineering, no. 32). New York: Marcel Dekker, 1996, pp. ix, 309 p.

[11]   D. T. Hallinan, M. G. De Angelis, M. G. Baschetti, G. C. Sarti, and Y. A. Elabd, "Water Transport in Proton Exchange Membranes: Insights from Time-Resolved Infrared Spectroscopy," (in English), *Ecs Transactions,* vol. 33, no. 1, pp. 1029-+, 2010, doi: 10.1149/1.3484596.

[12]   D. T. Hallinan Jr. and Y. A. Elabd, "Sorption and Diffusion Selectivity of Methanol/Water Mixtures in NAFION," in *Mini-Micro Fuel Cells*, S. Kakaç, A. Pramuanjaroenkij, and L. Vasiliev Eds., (NATO Science for Peace and Security Series C: Environmental Security: Springer Netherlands, 2008, ch. 13, pp. 189-208.

[13]   D. T. Hallinan Jr. and Y. A. Elabd, "Diffusion and sorption of methanol and water in naflon using time-resolved Fourier transform infrared-attenuated total reflectance spectroscopy," *Journal of Physical Chemistry B,* vol. 111, no. 46, pp. 13221-13230, Nov 22 2007, doi: 10.1021/jp075178n.

[14]   M. G. Baschetti, E. Piccinini, T. A. Barbari, and G. C. Sarti, "Quantitative analysis of polymer dilation during sorption using FTIR-ATR spectroscopy," *Macromolecules,* vol. 36, no. 25, pp. 9574-9584, Dec 16 2003, doi: 10.1021/ma0302457.

[15]   D. J. Buckley, M. Berger, and D. Poller, "The swelling of polymer systems in solvents. I. Method for obtaining complete swelling–time curves," *Journal of Polymer Science,* vol. 56, no. 163, pp. 163-174, 1962, doi: https://doi.org/10.1002/pol.1962.1205616314.

[16]   D. J. Buckley and M. Berger, "The swelling of polymer systems in solvents. II. Mathematics of diffusion," *Journal of Polymer Science,* vol. 56, no. 163, pp. 175-188, 1962, doi:

Soft Matter Accepted Manuscript

https://doi.org/10.1002/pol.1962.1205616315.

[17] W. A. Laftah and S. Hashim, "The influence of plant natural fibers on swelling behavior of polymer hydrogels," (in English), *J. Compos Mater.,* Article vol. 48, no. 5, pp. 555-569, Mar 2014, doi: 10.1177/0021998313476323.

[18] J. Gao *et al.*, "Synthesis and characterization of superabsorbent composite by using glow discharge electrolysis plasma," *Reactive and Functional Polymers,* vol. 68, no. 9, pp. 1377-1383, 2008/09/01/ 2008, doi: https://doi.org/10.1016/j.reactfunctpolym.2008.06.018.

[19] M. Shahinpoor, "Ionic Polymer Metal Composites (IPMCs) Smart Multi-Functional Materials and Artificial Muscles " in *Ionic Polymer Metal Composites*, vol. 1, M. Shahinpoor Ed., (RSC Smart Materials, no. 17), 2016, sec. Prefix, pp. V-VII.

[20] Y. Bar-Cohen, "Electroactive Polymers as Artificial Muscles: Capabilities, Potentials and Challenges," in *Robotics 2000*, 2000, pp. 188-196.

[21] J.-W. Lee and Y.-T. Yoo, "Anion effects in imidazolium ionic liquids on the performance of IPMCs," *Sensors and Actuators B: Chemical,* vol. 137, no. 2, pp. 539-546, 2009/04/02/ 2009, doi: https://doi.org/10.1016/j.snb.2009.01.041.

[22] M. Hao, Y. Wang, Z. Zhu, Q. He, D. Zhu, and M. Luo, "A Compact Review of IPMC as Soft Actuator and Sensor: Current Trends, Challenges, and Potential Solutions From Our Recent Work," (in English), *Frontiers in Robotics and AI,* Review vol. 6, no. 129, 2019-December-05 2019, doi: 10.3389/frobt.2019.00129.

[23]   B. Lopes and P. J. C. Branco, "Ionic polymer metal-composite (IPMC) actuators: Augmentation of their actuation force capability," in *2009 35th Annual Conference of IEEE Industrial Electronics*, 3-5 Nov. 2009 2009, pp. 1180-1184, doi: 10.1109/IECON.2009.5414659.

[24] Y. Bar-Cohen and I. A. Anderson, "Electroactive polymer (EAP) actuators—background review," *Mechanics of Soft Materials,* vol. 1, no. 1, p. 5, 2019/03/22 2019, doi: 10.1007/s42558-019-0005-1.

[25] G. M. Spinks *et al.*, "A novel "dual mode" actuation in chitosan/polyaniline/carbon nanotube fibers," *Sensors and Actuators B: Chemical,* vol. 121, no. 2, pp. 616-621, 2007/02/20/ 2007, doi: https://doi.org/10.1016/j.snb.2006.04.103.

[26] R. Kiefer, P. A. Kilmartin, G. A. Bowmaker, R. P. Cooney, and J. Travas-Sejdic, "Actuation of polypyrrole films in propylene carbonate electrolytes," *Sensors and Actuators B: Chemical,* vol. 125, no. 2, pp. 628-634, 2007/08/08/ 2007, doi: https://doi.org/10.1016/j.snb.2007.03.008.

[27] T. F. Otero, M. Marquez, and I. J. Suarez, "Polypyrrole: Diffusion coefficients and degradation by overoxidation," *The Journal of Physical Chemistry B,* vol. 108, no. 39, pp. 15429-15433, 2004.

[28] R. J. Young and P. A. Lovell, *Introduction to polymers*. CRC press, 2011.

[29] P. C. Hiemenz and T. P. Lodge, *Polymer chemistry*. CRC press, 2007.

[30] P. Zhao, B. Xu, Y. Zhang, B. Li, and H. Chen, "Study on the Twisted and Coiled Polymer Actuator with Strain Self-Sensing Ability," *ACS Applied Materials & Interfaces,* vol. 12, no. 13, pp. 15716-15725, 2020/04/01 2020, doi: 10.1021/acsami.0c01179.

[31] C. Lamuta, S. Messelot, and S. Tawfick, "Theory of the tensile actuation of fiber reinforced coiled muscles," *Smart Materials and Structures,* vol. 27, no. 5, p. 055018, 2018, doi: 10.1088/1361-665X/aab52b.

[32] C. S. Haines *et al.*, "Artificial Muscles from Fishing Line and Sewing Thread," *Science,* vol. 343, p. 868, 2014. [Online]. Available: https://science.sciencemag.org/content/343/6173/868.long.

[33] Z. Liu *et al.*, "Hierarchically buckled sheath-core fibers for superelastic electronics, sensors, and muscles," *Science,* vol. 349, no. 6246, pp. 400-404, 2015.

[34] P. Kotak, T. Weerakkody, and C. Lamuta, "Physics-based dynamic model for the electro-thermal actuation of bio-inspired twisted spiral artificial muscles (TSAMs)," *Polymer,* vol. 222, p. 123642, 2021/04/22/ 2021, doi: https://doi.org/10.1016/j.polymer.2021.123642.

[35]   Y. Kojima, A. Usuki, M. Kawasumi, A. Okada, T. Kurauchi, and O. Kamigaito, "Sorption of water in nylon 6-clay hybrid," *Journal of Applied Polymer Science,* vol. 49, no. 7, pp. 1259-1264, 1993, doi: https://doi.org/10.1002/app.1993.070490715.

[36]   M. D. Lima *et al.*, "Efficient, Absorption-Powered Artificial Muscles Based on Carbon Nanotube Hybrid Yarns," *Small,* vol. 11, no. 26, pp. 3113-3118, 2015, doi: https://doi.org/10.1002/smll.201500424.

[37]   P. J. Flory, *Principles of Polymer Chemistry*. Cornell University Press, 1953.

[38]   M. Quesada-Pérez, J. A. Maroto-Centeno, J. Forcada, and R. Hidalgo-Alvarez, "Gel swelling theories: the classical formalism and recent approaches," *Soft Matter,* vol. 7, no. 22, pp. 10536-10547, 2011.

[39]   W. M. Deen, *Analysis of transport phenomena* (Topics in chemical engineering). New York: Oxford University Press, 1998, pp. xix, 597 p.

[40]   D. T. Hallinan Jr., "Transport in polymer electrolyte membranes using time-resolved FTIR-ATR spectroscopy," Ph.D., Chemical and Biological Engineering, Drexel University, Philadelphia, 2009.

[41]   S. Chandrashekar, O. Oparaji, G. Yang, and D. Hallinan, "Communication—7Li MRI Unveils Concentration Dependent Diffusion in Polymer Electrolyte Batteries," *Journal of The Electrochemical Society,* vol. 163, no. 14, pp. A2988-A2990, January 1, 2016 2016, doi: 10.1149/2.0681614jes.

[42]   K. Ichikawa, T. Mori, H. Kitano, M. Fukuda, A. Mochizuki, and M. Tanaka, "Fourier transform infrared study on the sorption of water to various kinds of polymer thin films," *Journal of Polymer Science Part B: Polymer Physics,* vol. 39, no. 18, pp. 2175-2182, 2001, doi: https://doi.org/10.1002/polb.1191.

[43]   M. Métayer *et al.*, "Diffusion of water through various polymer films: a new high performance method of characterization," *Polymer Testing,* vol. 18, no. 7, pp. 533-549, 1999/10/01/ 1999, doi: https://doi.org/10.1016/S0142-9418(98)00052-X.

[44]   D. T. Hallinan, M. G. De Angelis, M. G. Baschetti, G. C. Sarti, and Y. A. Elabd, "Non-Fickian Diffusion of Water in Nafion," (in English), *Macromolecules,* vol. 43, no. 10, pp. 4667-4678, May 25 2010, doi: 10.1021/ma100047z.

[45]   B. Carnahan, H. A. Luther, and J. O. Wilkes, *Applied numerical methods*. New York: Wiley (in English), 1969.

[46]   T. F. Fuller and J. Newman, "Experimental Determination of the Transport Number of Water in Nafion 117 Membrane," *Journal of The Electrochemical Society,* vol. 139, no. 5, pp. 1332-1337, 1992/05/01 1992, doi: 10.1149/1.2069407.

[47]   J. Lin, P.-H. Wu, R. Wycisk, P. N. Pintauro, and Z. Shi, "Properties of water in prestretched recast Nafion," *Macromolecules,* vol. 41, no. 12, pp. 4284-4289, 2008.

[48]   T. A. Zawodzinski Jr *et al.*, "Water uptake by and transport through Nafion® 117 membranes," *Journal of the electrochemical society,* vol. 140, no. 4, p. 1041, 1993.

[49]   E. Stavrinidou, P. Leleux, H. Rajaona, M. Fiocchi, S. Sanaur, and G. G. Malliaras, "A simple model for ion injection and transport in conducting polymers," *Journal of Applied Physics,* vol. 113, no. 24, p. 244501, 2013/06/28 2013, doi: 10.1063/1.4812236.

[50]   J. Newman and K. E. Thomas-Alyea, *Electrochemical systems*. John Wiley & Sons, 2012.

[51]   F. e. Chakik, M. Kaddami, and M. Mikou, "Effect of operating parameters on hydrogen production by electrolysis of water," *International Journal of Hydrogen Energy,* vol. 42, no. 40, pp. 25550-25557, 2017/10/05/ 2017, doi: https://doi.org/10.1016/j.ijhydene.2017.07.015.

[52]   A. E. H. Love, "A treatise on the mathematical theory of elasticity, Dover Publications," *New York,* vol. 1, 1944.

[53]   C. Wu and W. Zheng, "A Modeling of Twisted and Coiled Polymer Artificial Muscles Based on Elastic Rod Theory," *Actuators,* vol. 9, no. 2, p. 25, 2020. [Online]. Available:

https://www.mdpi.com/2076-0825/9/2/25.

[54] G. M. Spinks, S. E. Bakarich, S. Aziz, B. Salahuddin, and H. Xin, "Using force-displacement relations to obtain actuation parameters from artificial muscles," *Sensors and Actuators a-Physical,* vol. 290, pp. 90-96, May 2019, doi: 10.1016/j.sna.2019.03.012.

[55] F. Karami and Y. Tadesse, "Modeling of twisted and coiled polymer (TCP) muscle based on phenomenological approach," *Smart Materials and Structures (Print),* vol. 26, no. 12, p. 12, 2017, doi: DOI:101088/1361-665X/aa8d7d.

[56] J. Brandrup, E. H. Immergut, and E. A. Grulke, Eds. *Polymer Handbook (4th Edition)*. John Wiley & Sons, 2003.

[57] J. B. Gluck-Hirsch and J. L. Kokini, "Determination of the molecular weight between crosslinks of waxy maize starches using the theory of rubber elasticity," *Journal of Rheology,* vol. 41, no. 1, pp. 129-140, 1997, doi: 10.1122/1.550804.

[58] S. J. Buwalda, K. W. Boere, P. J. Dijkstra, J. Feijen, T. Vermonden, and W. E. Hennink, "Hydrogels in a historical perspective: from simple networks to smart materials," *Journal of controlled release : official journal of the Controlled Release Society,* vol. 190, pp. 254-73, Sep 28 2014, doi: 10.1016/j.jconrel.2014.03.052.

[59] J. Crank, "A theoretical investigation of the influence of molecular relaxation and internal stress on diffusion in polymers," *Journal of Polymer Science,* vol. 11, no. 2, pp. 151-168, 1953, doi: https://doi.org/10.1002/pol.1953.120110206.

[60] R. Skouri, F. Schosseler, J. Munch, and S. Candau, "Swelling and elastic properties of polyelectrolyte gels," *Macromolecules,* vol. 28, no. 1, pp. 197-210, 1995, doi: 10.1021/ma00105a026.

[61] Y. Li and T. Tanaka, "Kinetics of swelling and shrinking of gels," *The Journal of Chemical Physics,* vol. 92, no. 2, pp. 1365-1371, 1990, doi: 10.1063/1.458148.

[62] V. A. Davankov and A. V. Pastukhov, "Paradoxes of thermodynamics of swelling equilibria of polymers in liquids and vapors," *The Journal of Physical Chemistry B,* vol. 115, no. 51, pp. 15188-15195, 2011.

[63] M. B. Satterfield and J. B. Benziger, "Non-Fickian Water Vapor Sorption Dynamics by Nafion Membranes," *The Journal of Physical Chemistry B,* vol. 112, no. 12, pp. 3693-3704, 2008/03/01 2008, doi: 10.1021/jp7103243.

[64] G. Marom, "Swelling and hygroelasticiiy of polymeric composites," *Polymer Engineering & Science,* vol. 17, no. 11, pp. 799-802, 1977, doi: https://doi.org/10.1002/pen.760171107.

[65] E. M. Davis, C. M. Stafford, and K. A. Page, "Elucidating Water Transport Mechanisms in Nafion Thin Films," *ACS Macro Letters,* vol. 3, no. 10, pp. 1029-1035, 2014/10/21 2014, doi: 10.1021/mz500515b.

[66] M. Rubinstein and R. H. Colby, *Polymer physics*. Oxford university press New York, 2003.

[67] X. Hu *et al.*, "Fast Large-Stroke Sheath-Driven Electrothermal Artificial Muscles with High Power Densities," *Advanced Functional Materials,* p. 2200591, 2022.

[68] J. Mu *et al.*, "Sheath-run artificial muscles," *Science,* vol. 365, no. 6449, pp. 150-155, 2019, doi: 10.1126/science.aaw2403.